

**Rate theory description of atomic stick-slip friction**Danny Perez,<sup>1</sup> Yalin Dong,<sup>2</sup> Ashlie Martini,<sup>2</sup> and Arthur F. Voter<sup>1</sup><sup>1</sup>*Theoretical Division T-1, Los Alamos National Laboratory, Los Alamos, New Mexico 87545, USA*<sup>2</sup>*School of Mechanical Engineering, Purdue University, 585 Purdue Mall, West Lafayette, Indiana 47907, USA*

(Received 8 April 2010; published 10 June 2010)

We assess the validity of assumptions that underpin common low-dimensional rate theory descriptions of nanoscale stick-slip friction by completely specifying harmonic transition state theory kinetic parameters from an atomistic model. The resultant kinetic model is able to reliably reproduce the temperature and velocity dependence of friction as obtained by direct fully atomistic accelerated molecular-dynamics simulations. Analysis of the parameters extracted from the model indicates that, while energetics of the transition pathways can be adequately captured by low-dimensional effective Hamiltonians, rate theory prefactors contain inherently high-dimensional entropic contributions that cannot be accounted for. Despite these limitations, we show that simplified models can still be sufficiently robust to capture the prominent features of stick-slip friction.

DOI: [10.1103/PhysRevB.81.245415](https://doi.org/10.1103/PhysRevB.81.245415)

PACS number(s): 83.10.Rs

**I. INTRODUCTION**

Atomic stick-slip friction has been an area of extreme interest both from the fundamental science and engineering application perspectives; of particular focus has been characterization of its velocity and temperature dependence. Experimental studies have shown that mean friction is significantly affected by both velocity (see, for example, Refs. 1–3) and temperature (see, for example, Refs. 4–6). However, the exact form of these relationships is still a subject of debate and an understanding of their underlying physics remains imperfect. Modeling efforts employed to investigate these physical mechanisms can be broadly divided into two approaches: direct, fully atomistic models [i.e., molecular-dynamics (MD) simulations such as those employed in Refs. 5 and 7–9] and reduced-order, rate-based approximations (i.e., Tomlinson-type models such as those described in Refs. 10–13); the former typically being used to elucidate the atomistic detail of the process while the latter is relied upon to provide analytical guidelines to assist in the interpretation of measurements. Indeed, an advantage of rate theory-based models is that they enable one to make predictions over experimentally relevant time and length scales that are often inaccessible to direct MD simulations.

Two rate theory-based models are particularly relied upon to interpret simulations and experiments. First, at low temperatures and/or high velocities, the ramped creep model of Sang *et al.*<sup>10</sup> predicts—under the assumptions that most slips occur very close to the instability point, that backslips do not occur and that the slip dynamics can be well described by a one-mass one-spring Tomlinson Hamiltonian—that the average friction force should go as

$$F \propto \text{const} - T^{2/3} |\ln v/T|^{2/3}, \quad (1)$$

where  $T$  is the temperature and  $v$  the scanning velocity. At the other end of the spectrum—in the limit of high temperatures and low velocities—Krylov, Frenken *et al.* predict that, when the temperature and driving velocities are such that the system is close to thermal equilibrium at all times, the system should eventually enter a so-called thermal drift (TD)

regime wherein the friction force is very small and varies as<sup>12,13</sup>

$$F \propto \frac{v}{T} \exp(1/T), \quad (2)$$

assuming that the slip rate prefactor can be considered independent of the cantilever's support position. Both these models are perceived as providing an adequate description of the relevant physics needed to characterize the temperature and velocity dependence of friction.

However, a rigorous justification of the general applicability and robustness of these models is still lacking. Specifically, the extent to which the simplified low-dimensional Hamiltonians can adequately describe even highly idealized, many-dimensional systems has not been thoroughly assessed. In the present work, we bridge the gap between the two approaches by completely specifying model parameters using information obtained from a fully atomistic system and numerically solving the resulting equations. By comparing with fully dynamical atomistic simulations, we are able to provide a direct assessment of the applicability of rate theory to more complex and realistic conditions. Doing so, we demonstrate that parameter-free kinetic models based on harmonic transition state theory (HTST) are able to reproduce the temperature and velocity dependence of friction as obtained by direct atomistic simulations to within a few percent over a wide range of conditions. By comparing with the aforementioned models, we also find that the use of simplified Hamiltonians is not justified in general, primarily because the rate prefactors contain nontrivial many-dimensional contributions. But despite these limitations, in the particular case of interest here, the simplified models (ramped creep and TD) are sufficiently robust to account for the significant features of stick-slip friction over most of the temperature and velocity ranges to which they are applicable.

**II. METHODOLOGY**

The atomistic model we use (cf. Fig. 1) is meant to mimic the contact of an elastically compliant Cu (111)-terminated

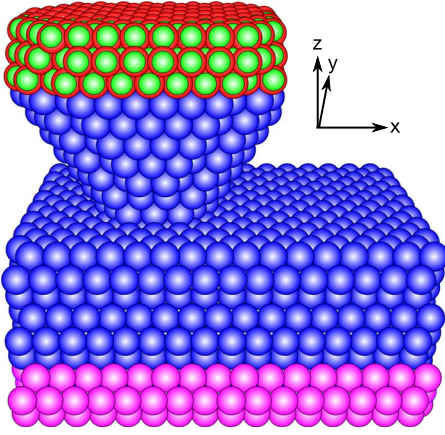


FIG. 1. (Color online) Atomistic configuration used in the present study. Pink atoms (bottom three layers) are fixed and red atoms (top three layers) are tied one-to-one to the green support atoms (smaller atoms in the top three layers). Blue atoms (middle) are unconstrained.

friction force microscope tip with an infinite Cu (111) surface. In order to keep the number of atoms at a minimum, the cantilever and much of the tip are not explicitly present but are taken into account using an effective model where the top three layers of atoms are coupled one-by-one to virtual atoms through a harmonic potential with spring constant  $k_s = 0.5 \text{ eV}/\text{\AA}^2$ . Using this procedure, only 3337 atoms need to be considered explicitly. The lattice of virtual atoms (the support) is rigid and is free to move only along the  $z$  direction. During the simulation, the support is uniformly translated at scanning velocity  $v$  along the  $x$  ( $\bar{1}01$ ) direction. The bottommost three layers of the surface are held fixed and periodic boundary conditions are applied in  $x$  and  $y$ . The nonvirtual atoms in the system interact through an embedded atom model fitted to Cu.<sup>14</sup> Canonical dynamics are obtained using a Langevin thermostat applied to atoms found at least three layers away from the contact; other atoms evolve under Newtonian dynamics. The contact is hexagonal in shape and contains 19 atoms. Atomistic simulations are carried out using the parallel replica dynamics method,<sup>15,16</sup> which we recently showed was able to provide 100- to 1000-fold speedups over conventional MD for this type of system, enabling one to reliably reproduce experimentally observed trends.<sup>17</sup>

Despite its very small size, our model should adequately account for friction force measurements in the limit of very stiff cantilevers, where the elasticity of the tip apex is the dominant deformation mode.<sup>18</sup> In this limit, the tip base (i.e., the support in our terminology) can be considered fixed at its cantilever-imposed position. Complications related to coupling of the slow cantilever and fast contact dynamics are thus avoided.<sup>18,19</sup>

The corresponding kinetic model consists of a set of master equations to compute the probability  $p$  that the system resides in any of the  $N(t)$  available potential energy wells (or, equivalently, in any of the possible atomistic configurations of the contact) available at a given support position  $x_s(t)$ . For simplicity, we assume (as validated by atomistic simulations in the temperature and time scale ranges of interest here) that the only relevant transitions are single forward slips and

backslip. Using the standard form for a system with time-dependent rates, one obtains

$$\frac{\partial p_i(t)}{\partial t} = \sum_{j=1}^{N(t)} k_{j \rightarrow i}(t) p_j(t) - k_{i \rightarrow j}(t) p_i(t), \quad (3)$$

where  $k_{i \rightarrow j}(t)$  is the instantaneous transition rate from state  $i$  to state  $j$  when the support is located at  $x_s(t)$ . Once the time-dependent probabilities of occupation of each state are determined, statistical quantities are obtained as weighted averages over the different states.

The minimum-energy pathways connecting all  $N(x_s)$  states for every  $x_s$  and the associated transition states were obtained using the string method.<sup>20</sup> With these, the transition rates are computed within multidimensional HTST,<sup>21</sup> where they are given by the product of a temperature-independent prefactor  $\nu_0$  and a temperature-dependent activation term, of the form

$$k_{i \rightarrow j} = \left[ \frac{\prod_{k=1}^M \nu_i^k}{\prod_{k=1}^{M-1} \nu_{i-j}^{k*}} \right] \exp \left[ - \frac{\Delta E_{i \rightarrow j}}{k_B T} \right]. \quad (4)$$

The activation energy  $\Delta E_{i \rightarrow j}$  is the difference between the energy of the system at the transition state between  $i$  and  $j$  and that at the minimum  $i$ , and  $\nu$  and  $\nu^*$  are the real vibrational eigenfrequencies at the minimum and saddle, respectively. The frequencies were obtained by direct diagonalization of Hessian matrices obtained by finite differences. By carrying out this procedure we determined that only between 1 and 3 states are available to the system at any given time (see below); these states will be indexed 0, 1/2, 1, corresponding to fcc, hcp, or translated fcc registry between tip and surface, respectively. Once the rates are fully specified using Eq. (4), Eq. (3) is numerically integrated over one period of the surface potential with a specified velocity and initial condition  $p_0=1$ ,  $p_{1/2}=p_1=0$  [since  $x_s(0)$  is chosen so that 0 is the only stable state] and relevant statistical averages computed.

### III. RESULTS

Figures 2 and 3 summarize the parameters extracted from the atomistic model. First, the  $T=0 \text{ K}$  lateral friction forces are on the order of 1 nN and exhibit the characteristic sawtooth pattern, which is experimentally typical. The energies along the branches also show that the hcp 1/2 state is disfavored because it entails a bending of the tip along the  $y$  direction and is thus accessible from a narrower range of support positions compared to the fcc 0 and 1 branches. Despite this, there is significant overlap between branches 1/2 and either 0 or 1; the three branches are even simultaneously stable, albeit on a very narrow range of support positions around  $x_s = 1.2 \text{ \AA}$ .

Figure 3 shows the evolution of the barrier height and prefactor entering in Eq. (4) with variation in the support position for slips from branch 0 to branch 1/2 (other slips and backslips exhibit the same qualitative behavior). When branch 1/2 first becomes stable (around  $x_s = 0.44 \text{ \AA}$ ), the slip barrier  $\Delta E$  is fairly high (about 0.9 eV) but it decays steadily

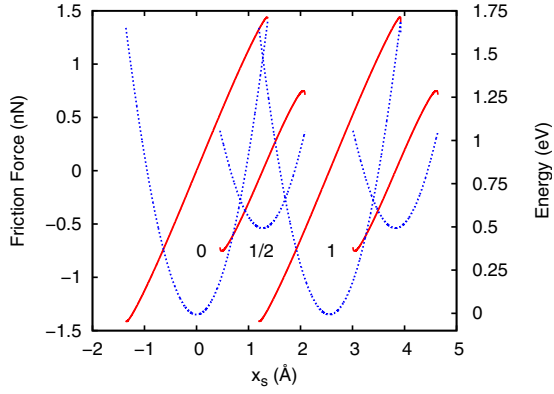


FIG. 2. (Color online) Friction force (red continuous line, left axis) and energy (blue dotted line, right axis) along different branches as a function of the support position  $x_s$  at  $T=0$  K.

and finally vanishes around  $x_s^* = 1.38$  Å. At this point, branch 0 is unstable (there is at least one normal mode with an imaginary frequency) and slip to branch 1/2 becomes a spontaneous process. Analysis shows that  $\Delta E \propto (1 - x_s/x_s^*)^{3/2}$  close to  $x_s^*$ , in agreement with a first-order expansion of a one-dimensional (1D) Tomlinson-type potential.<sup>10</sup> This agreement is expected since, for simple slips, a one-spring effective Hamiltonian should contain the essential ingredients to approximate the energetics.

Interestingly, the positional dependence of the prefactor differs significantly from the 1D prediction,<sup>10</sup>  $\nu_0 \propto (1 - x_s/x_s^*)^{1/2}$ . Instead,  $\nu_0$  is well approximated by the functional form  $e^{-x_s/x_s^*} (1 - x_s/x_s^*)^c$  with  $c \approx 0.4$ . It is tempting to associate the power-law decay solely to the softening of the minimum mode whose frequency vanishes as  $x_s \rightarrow x_s^*$ , in analogy to the 1D case. However, a fit to the frequency of that mode shows a power-law behavior with an exponent of about 0.1 in  $(1 - x_s/x_s^*)$ ; the observed decrease in the prefactor is rather a collective effect with significant contributions from a number of minimum and transition state modes, reflecting a complex change in the shape of the energy landscape as the minimum destabilizes.

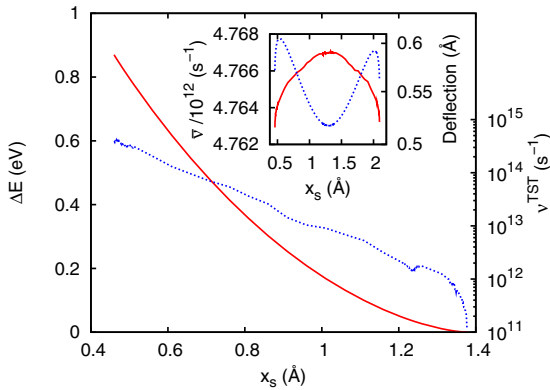


FIG. 3. (Color online) Energy barrier (red continuous line, left axis) and prefactor for slip (blue dotted line, right axis) between branches 0 and 1/2 as a function of support position. Inset: geometric average of the vibration frequencies (red continuous line, left axis) and deflection of the tip (blue dotted line, right axis) for state 1/2 as a function of support position.

The apparently exponential background at smaller  $x_s$  also stems from the inherently multidimensional nature of the system. While it is difficult to unambiguously isolate different contributions, there is reason to believe that strain contributes significantly to the large change in prefactor. Indeed, it is now well appreciated that elastic deformation can localize at the apex of the tip.<sup>18</sup> This in turn causes the softening of the strained material due to anharmonic effects (akin to the strain dependence of elastic constants) and a decrease in its vibrational frequencies. As shown in the inset of Fig. 3, changes in the average vibrational frequency correlate very well with the amount of deflection of the tip (the distance between the center of mass of the contact at a given  $x_s$  and its elastic equilibrium position for a free tip), except very close to the instability points of branch 1/2 ( $x_s \approx 0.5$  Å and  $x_s \approx 2$  Å) where the average frequency drops despite a decrease in deflection due to the presence of soft modes, as discussed above. While the absolute change in each frequency is very modest (around 0.1%), frequencies enter multiplicatively in Eq. (4) so that very slight differences in the strain state of the system between the minimum and the transition state can easily account for the observed 100-fold variation in prefactor. In the present case, the contributions combine to yield an approximately exponential variation but, in general, more complex nonmonotonic behaviors cannot be excluded. Another surprising feature of the results is the very large magnitude of the prefactor, which varies between about 100 THz for small  $x_s$  and 1 THz close to  $x_s^*$ . This is not totally unexpected as it was previously pointed out that apex modes of sharp tips possess high vibrational frequencies that can couple efficiently with the activation pathway for slip; however, based on these arguments, prefactors were postulated to be in the gigahertz range and not in the terahertz as shown here.<sup>18</sup>

To put these results in perspective, it is instructive to compare our atomistic results with a simplified 1D model proposed in Ref. 18, where the Hamiltonian of the surface/tip/cantilever system is approximated by an  $N$ -mass,  $N$ -spring generalization of the conventional Tomlinson Hamiltonian,

$$H = \frac{1}{2} \sum_{i=1}^N m_i v_i^2 + \frac{E_0}{2} [1 - \cos(2\pi x_i)] + \frac{1}{2} \sum_{i=1}^{N-1} k_i (x_{i+1} - x_i)^2 + \frac{1}{2} k_s (x_s - x_N)^2. \quad (5)$$

In this model, the tip and cantilever are discretized into  $N$  particles. Each particle interacts with its neighbors through springs that modulate shear deformation; in addition, the first particles interact with a surface through a cosine corrugation potential and the last is tied to a fixed support located at  $x_s$  via a spring of stiffness  $k_s$  that accounts for the elasticity of the cantilever. This Hamiltonian is designed to take into account the finite compliance of the tip and cantilever as well as their respective masses. Here, we choose  $N=1000$  (enough to capture proper apex deformation of the tip),  $k_i = (i+i_0)^2 k$ , and  $m_i = (i+i_0)^2 m$  (mass and stiffness proportional to the cross-section of the tip at a given position) except for the cantilever mass and stiffness which are taken to be  $m_N$

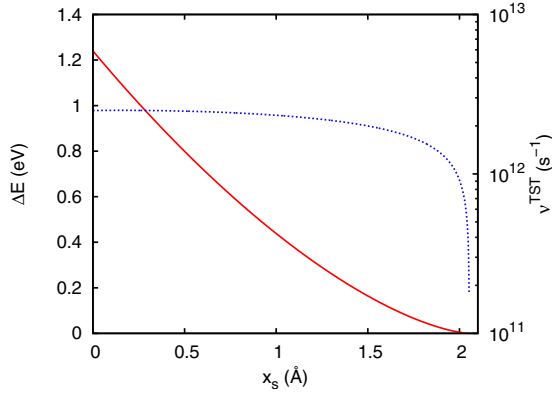


FIG. 4. (Color online) Energy barrier (red continuous line, left axis) and prefactor for slip (blue dotted line, right axis) as a function of support position for the simplified  $N$ -mass  $N$ -spring Hamiltonian.

$=10^{18} m$  and  $k_s=1000$  N/m, respectively. The remaining constants were selected to correspond loosely to our atomistic system:  $k=0.5$  eV/Å<sup>2</sup>,  $E_0=1$  eV,  $i_0=3$ , and  $m$  is taken to be the mass of a Cu atom. So parameterized, the vibrational frequencies of the tip/cantilever subsystem—from about 32 KHz for the cantilever oscillation mode to 3.5 THz for apex bending modes—are compatible with typical experimental values. Using this Hamiltonian, we repeated the characterization procedure described above and computed the slip barrier and prefactor as a function of the support position  $x_s$ .

The results, reported in Fig. 4, show that the slip barriers again vary approximately as  $(1-x_s/x_s^*)^{3/2}$ , in agreement with the atomistic results. Also in qualitative agreement with the atomistic results, the slip prefactor is observed to be in the terahertz range and to drop as the instability point is reached. The prefactor is so high because the unstable saddle mode corresponding to slip is almost totally orthogonal to the slow cantilever normal mode and is instead mainly localized in the first few layers of the tip; it is thus insensitive to the mass and stiffness of the cantilever and is instead controlled by the effective stiffness of the apex and by the curvature of the corrugation potential. Note that for soft cantilevers and stiff tips this decoupling can break down leading to very low prefactors. This will be investigated in detail elsewhere.

These results strongly suggest that the very high prefactors obtained from our small-scale atomistic model are representative of fully coupled surface/tip/cantilever systems for stiff enough cantilevers and are not an artifact of the small size of the system. They also support the anharmonic origin of the exponential background observed for the atomistic system, as this contribution is absent from the purely harmonic results.

In order to validate the kinetic model, we compare its predictions with direct atomistic parallel replica dynamics simulation; these results are reported in Fig. 5. The simulations agree with the model within the statistical error bars (a few percent) over four orders of magnitude in velocity and over temperatures ranging from cryogenic to ambient. This clearly demonstrates the ability of a HTST-based master-equation model to quantitatively predict atomic stick-slip be-

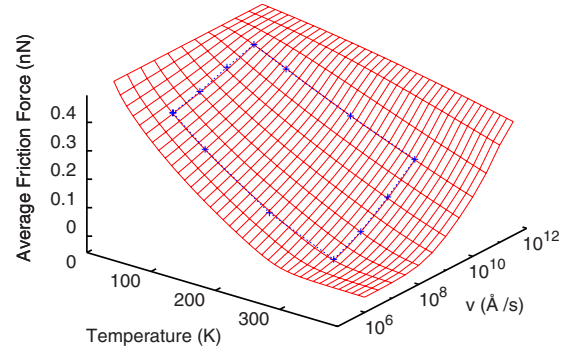


FIG. 5. (Color online) Average friction force as a function of temperature and scanning velocity  $v$ . Red surface: kinetic model; blue symbols and dotted line: atomistic parallel replica dynamic simulations. Error bars on the atomistic results are comparable to the symbol size.

havior over a wide range of conditions. Note that this level of agreement requires the consideration of the temperature dependence of the canonical average of the friction forces (obtained by direct MD simulation at different temperatures and support positions). Qualitatively, the results properly reproduce the expected limiting behaviors, on the one hand, at very low temperatures and/or high velocities, the system is essentially pushed all the way up to the instability point before slip occurs. In this case, the friction force converges to its ultimate  $T=0$  K limit,  $F=F^0$ . On the other hand, at high temperatures and/or low velocities, the system remains close to equilibrium and the friction vanishes. The relatively high scanning velocity at which this regime sets in is expected given the high effective stiffness of our system; for an infinite stiffness, the average friction force would be zero at any velocity or temperature. In between these two limits, the behavior of the force is nontrivial; this will now be considered in more detail.

Figure 6 reproduces a few constant velocity curves as obtained by the kinetic model. The behavior of the force reflect the limits discussed above, at low temperatures, slips only occur close to the instability point and the force saturates at its limiting value  $F^0 \approx 0.49$  nN while at high enough temperatures, thermal quasiequilibrium prevails and the friction force vanishes. As discussed in Sec. I, in the intermediate regime where the temperature is low enough and velocities are large enough that slips occur late and backslips are improbable, the ramped creep model should presumably apply. The top inset of Fig. 6 demonstrates that the low-temperature forces approximately follow the temperature and velocity scaling implied by Eq. (1). This is easily understood given that the assumptions of the model [ $\Delta E \propto (1-x_s/x_s^*)^{3/2}$  and  $\bar{\nu} \propto (1-x_s/x_s^*)^{1/2}$ ] are reasonably representative, albeit somewhat accidentally, of the atomistic energy landscape insofar as slips occur close to  $x_s^*$ . As the temperature is raised, slips occur on average at smaller values of  $x_s$  and the exponential background of  $\nu_0$  affects the resulting force to a larger extent. But overall the predictions of the model are robust against these perturbations and offer an adequate description of the results of the kinetic model down to very small forces.

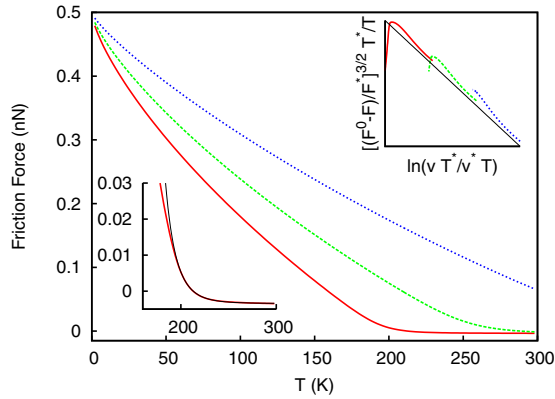


FIG. 6. (Color online) Average friction force as a function of temperature for different scanning velocities, as inferred from the kinetic model. Red continuous line:  $10^4$  Å/s; green dashed line:  $10^6$  Å/s; blue dotted line:  $10^8$  Å/s. Bottom inset: blowup of the high-temperature region. The thin black line is a high-temperature fit to Eq. (2). Top inset: ramped creep scaling plot.  $T^*$ ,  $v^*$ , and  $F^*$  are arbitrary constants. The thin black line is a guide to the eyes and shows the expected ramped creep scaling [cf. Eq. (1)]. See text for detail.

For low enough velocities and high enough temperatures, backslips do occur at a significant rate and the system approaches thermal equilibrium at each  $x_s$ ; the ramped creep regime is then expected to break down and the low friction TD regime to prevail. In this limit, Eq. (2) should apply; this is indeed observed (cf. bottom inset of Fig. 6), albeit over an extremely limited range: in the present condition, it is restricted to forces below about 0.02 nN. This limited validity presumably stems from the very large variations in the slip rate prefactor with  $x_s$  which were not considered in deriving Eq. (2).

Interestingly, the force trace in the TD (not shown) regime is very similar to that of the quasiregular stick-slip ramped creep regime. Indeed, while the average friction vanishes, the maximal force observed along the trace is still about 0.6 nN and the characteristic sawtooth pattern is maintained. The only tell-tale sign of the TD regime is the presence of a small number of backslips close to  $x_s^*$ . A consequence of this observation is that, in practice, the TD regime does not strictly require scanning velocities such that  $\Delta/v \gg [\min_{i,j,x_s} k_{i \rightarrow j}(x_s)]^{-1}$ —with  $\Delta$  the period of the corrugation potential—for all  $x_s$ , only that it is so for the values of  $x_s$  where the probability to occupy a state (branch) other than the dominant one is not vanishingly small so that the latter contributes significantly to the average force. For example, at 300 K,  $k_{0 \rightarrow 1/2}$  can be as low as  $1 \text{ s}^{-1}$  for some values of  $x_s$ ; however, already by  $v=10^6$  Å/s, the friction is negligible.

The TD regime can thus be accessible at higher velocities than what a strict quasiequilibrium condition would suggest.

As both the ramped creep and TD formalisms consider both  $T$  and  $v$  as dynamical variables, the analysis of our results under velocity variations provides similar insights. Again, the ramped creep and the TD regimes are observed at large velocities and low velocities, respectively. Taken together, they cover most of the velocity and temperature range under the present conditions.

#### IV. CONCLUSION

In conclusion, we have demonstrated that a parameter-free HTST-based kinetic model is able to reproduce the temperature and velocity variation in the friction force as obtained from fully dynamical atomistic simulations with very high accuracy over a wide range of conditions. For the system considered here, the behavior is in reasonable agreement with that of a simple one-dimensional Tomlinson-type model close to the branch instability points. Because of that agreement, the ramped creep model adequately describes the variation in the friction force for all but the smallest values whereas the TD model properly accounts for the decay of that force. Our work, however, indicates that, due to the complex multidimensional nature of real systems, there is reason to expect that 1D models cannot be generally used as surrogates for atomically resolved systems, in particular, because the prefactors of the slip rates can be significantly influenced by intrinsically multidimensional effects.

While we demonstrated that rate theory can be successfully used to predict the friction force of reasonably realistic models, its range of direct applicability is limited to fairly stiff cantilevers. When that condition is not met, the dynamics of the contact and cantilever can be coupled on very long time scales due to the considerable inertia of the latter.<sup>18,19</sup> In this case, rate theory needs to be augmented by a proper dynamical model that couples tip and cantilever motion. This work is underway.

#### ACKNOWLEDGMENTS

Work at Los Alamos National Laboratory (LANL) was supported by the United States Department of Energy (U.S. DOE), Office of Basic Energy Sciences, Materials Sciences and Engineering Division. D.P. graciously acknowledges support from Canada's NSERC. A.M. and Y.D. are grateful to R. W. Carpick and Q. Li for helpful discussions and to the National Science Foundation for its support via Award No. CMMI-0758604. LANL is operated by Los Alamos National Security, LLC, for the National Nuclear Security Administration of the U.S. DOE under Contract No. DE-AC52-06NA25396.

<sup>1</sup>R. Bennewitz, T. Gyalog, M. Guggisberg, M. Bammerlin, E. Meyer, and H.-J. Güntherodt, *Phys. Rev. B* **60**, R11301 (1999).

<sup>2</sup>E. Gnecco, R. Bennewitz, T. Gyalog, C. Loppacher, M. Bammerlin, E. Meyer, and H.-J. Güntherodt, *Phys. Rev. Lett.* **84**,

1172 (2000).

<sup>3</sup>A. S. Enrico Gnecco, R. Bennewitz, and E. Meyert, *Wear* **254**, 859 (2003).

<sup>4</sup>A. Schirmeisen, A. L. Jansen, H. Hölscher, and H. Fuchs, *Appl.*

- Phys. Lett.* **88**, 123108 (2006).
- <sup>5</sup>R. M. J. Brukman, G. Gao, and J. A. Harrison, *J. Phys. Chem. C* **112**, 9358 (2008).
- <sup>6</sup>X. Zhao, S. R. Phillpot, W. G. Sawyer, S. B. Sinnott, and S. S. Perry, *Phys. Rev. Lett.* **102**, 186102 (2009).
- <sup>7</sup>M. D. Perry and J. A. Harrison, *J. Phys. Chem.* **99**, 9960 (1995).
- <sup>8</sup>M. R. Sørensen, K. W. Jacobsen, and P. Stoltze, *Phys. Rev. B* **53**, 2101 (1996).
- <sup>9</sup>Q. Zhang, Y. Qi, L. G. Hector, T. Cagin, and W. A. Goddard, *Phys. Rev. B* **72**, 045406 (2005).
- <sup>10</sup>Y. Sang, M. Dubé, and M. Grant, *Phys. Rev. Lett.* **87**, 174301 (2001).
- <sup>11</sup>E. Riedo, E. Gnecco, R. Bennewitz, E. Meyer, and H. Brune, *Phys. Rev. Lett.* **91**, 084502 (2003).
- <sup>12</sup>S. Y. Krylov, K. B. Jinesh, H. Valk, M. Dienwiebel, and J. W. M. Frenken, *Phys. Rev. E* **71**, 065101(R) (2005).
- <sup>13</sup>K. B. Jinesh, S. Y. Krylov, H. Valk, M. Dienwiebel, and J. W. M. Frenken, *Phys. Rev. B* **78**, 155440 (2008).
- <sup>14</sup>P. L. Williams, Y. Mishin, and J. C. Hamilton, *Modell. Simul. Mater. Sci. Eng.* **14**, 817 (2006).
- <sup>15</sup>A. F. Voter, *Phys. Rev. B* **57**, R13985 (1998).
- <sup>16</sup>B. P. Uberuaga, S. J. Stuart, and A. F. Voter, *Phys. Rev. B* **75**, 014301 (2007).
- <sup>17</sup>A. Martini, Y. Dong, D. Perez, and A. F. Voter, *Tribol. Lett.* **36**, 63 (2009).
- <sup>18</sup>S. Y. Krylov, J. A. Dijksman, W. A. van Loo, and J. W. M. Frenken, *Phys. Rev. Lett.* **97**, 166103 (2006).
- <sup>19</sup>S. Maier, Y. Sang, T. Filleter, M. Grant, R. Bennewitz, E. Gnecco, and E. Meyer, *Phys. Rev. B* **72**, 245418 (2005).
- <sup>20</sup>W. E. W. Ren, and E. Vanden-Eijnden, *Phys. Rev. B* **66**, 052301 (2002).
- <sup>21</sup>J. Vineyard, *J. Phys. Chem. Solids* **3**, 121 (1957).